THE BELL SYSTEM TECHNICAL JOURNAL
Vol. 56, No. 6, July–August 1977
Printed in U.S.A.

Characteristics of a Broadband Microwave Corrugated Feed: A Comparison Between Theory and Experiment

By C. DRAGONE

(Manuscript received December 14, 1976)

A corrugated feed with nearly ideal radiation characteristics from 17 GHz to 29 GHz has been built using a novel fabrication technique. The bandwidth of single-mode operation was maximized by properly choosing the input parameters of the feed. As a result, only the fundamental mode can propagate at the input from 19 GHz to 28.8 GHz. In this frequency range, the far field is essentially polarized in one direction. At frequencies higher than 28.8 GHz, there is a cross-polarized component caused by an unwanted mode. An approximate calculation of the power in this mode is given. A simple formula for the input reflection coefficient is provided. Results are included that show how to compute mode conversion in a conical taper, cross polarization from a corrugated horn, including contributions from spurious modes, and the reflection coefficient from the smooth-guide to corrugated-guide transition. Comparison of theory and experiment shows good agreement.

I. INTRODUCTION

It has been shown by Thomas[1] that under certain conditions the field over the aperture of a corrugated feed is virtually constant over a very wide frequency range. For this behaviour to occur, the radius a of the aperture must be much larger than a wavelength, i.e.,

$$ka \gg 1 \left(k = \frac{2\pi}{\lambda}\right) \tag{1}$$

and furthermore, the aperture must be illuminated by a single mode. If both conditions are satisfied, we can show that the field distribution is essentially independent of the surface reactance of the corrugated horn wall, X_s, and, as a consequence, it is little affected by the variation of X_s with frequency. This result is very important, for it implies that it

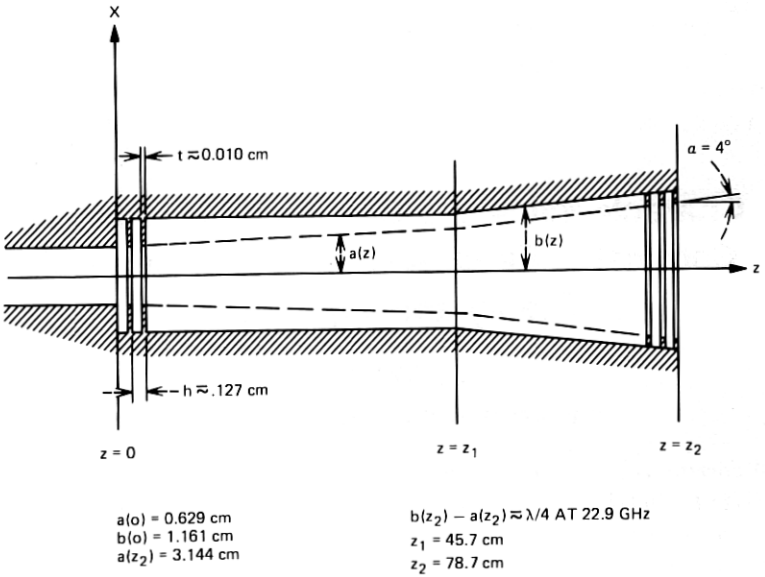

Fig. 1—Dimensions of the corrugated horn.

is possible to design a feed so that its radiation pattern is circularly symmetric and polarized in one direction over a very wide frequency range[1–3] (an octave or more). The most difficult condition to satisfy to obtain such large bandwidth is the requirement that a single mode be excited in the feed. This requirement is discussed in a separate article.[4] Here, after summarizing certain results of that article, we describe the results of an experiment. A long feed, with a flare angle of only 4°, was fabricated using a special technique described in Appendix D. At the input of the feed, which is shown in Fig. 1, the waveguide dimensions (the corrugated depth l and the radius a; see Fig. 1) were optimized so as to maximize the bandwidth of single mode propagation. As a consequence, unwanted modes were cut off (at the input) over the frequency range

$$\omega_1 < \omega < 1.6839\omega_1, \tag{2}$$

where $\omega_1 = 19$ GHz and $1.6839\omega_1 = 28.8$ GHz. The input reflection and the far field were then measured from 17 GHz to 35 GHz. The input reflection agrees very well with a simple formula given in eq. (42) and derived in Ref. 4. Over the frequency range (2), the far field is essentially polarized in one direction. At frequencies higher than 28.8 GHz, however, a strong cross-polarized component is caused by an unwanted HE'_{11} mode, which is excited primarily at the input of the feed. A simple expression for the power converted into this mode is given in Ref. 4.

II. PRELIMINARY CONSIDERATIONS

In the experiment described in Section V, the feed is excited at the input by a linearly polarized TE_{11} mode. Therefore, consideration will be restricted to the modes arising for this particular excitation.[2–8]

Consider a disk-loaded waveguide centered around the z axis as in Fig. 1, and let r, ϕ, z be cylindrical coordinates defined by $x = r\cos\phi$ and $y = r\sin\phi$. Assume for the moment that the waveguide parameters h, a, b, and t are independent of z. The separation h of the disks, which occupy the region $a < r < b$, is assumed to be much smaller than a wavelength λ

$$kh \ll 1. \tag{3}$$

The region between two consecutive disks forms a radial line whose input reactance jX at $r = a$ is a function of the radial length $l = b - a$; for $ka \gg 1$,

$$jX \approx jZ_0 \tan kl, \tag{4}$$

where $Z_0 = \sqrt{\mu_0/\epsilon_0}$. Because of condition (3), the effect of the disks can be adequately accounted for by introducing an effective surface reactance[2]

$$jX_s = jX\left(1 - \frac{t}{h}\right), \tag{5}$$

where t is the thickness of the disks, and by requiring that the field for $r < a$ satisfy the boundary conditions

$$\left.\begin{aligned} E_\phi &\approx 0 \\ H_\phi &\approx -\frac{E_z}{jX_s} \end{aligned}\right\} \text{ for } r = a, \tag{6}$$

where E_ϕ, H_ϕ, E_z are the ϕ and z components of the electric and magnetic field.

2.1 The HE_{lm} and HE'_{lm} modes

The properties of the hybrid modes[2–8] of a corrugated waveguide are determined by the radius a and the surface reactance X_s of the waveguide. In general, there is no simple relation[2] between the propagation constant β of a mode and the two parameters a and X_s. If, however, condition (1) is satisfied and furthermore

$$\frac{\nu}{ka} \ll 1, \tag{7}$$

where

$$y = -\frac{Z_0}{X_s}, \tag{8}$$

then we can show[2,4] that for all the modes except one, described in Appendix B of Ref. 4, the propagation constant is independent of X_s and is simply given by

$$\beta a \approx \sqrt{(ka)^2 - u^2}, \tag{9}$$

where u is a constant that is either the mth root of $J_0(u) = 0$, or of $J_2(u) = 0$. Thus, either

$$u = u_m, J_0(u_m) = 0 \tag{10}$$

or

$$u = u'_m, J_2(u'_m) = 0. \tag{11}$$

The modes to which eq. (10) applies will be called HE_{lm} modes and those corresponding to eq. (11), HE'_{lm} modes. The HE_{lm} modes approach asymptotically, for large ka, the field distribution[2,4]

$$\mathbf{E} = J_0\left(\frac{r}{a}u\right) e^{-j\beta z}\,\mathbf{i}_x, \tag{12}$$

whereas the HE'_{lm} modes approach the distribution

$$\mathbf{E} = J_2\left(\frac{r}{a}u\right)(\cos 2\phi \mathbf{i}_x + \sin 2\phi \mathbf{i}_y)e^{-j\beta z}. \tag{13}$$

The absence of a z component in eqs. (12) and (13) is due to the fact that this component vanishes like $1/ka$, as $ka \to \infty$.

The HE_{lm} modes, which are given by eq. (12), have the important property that the electric field is polarized in one direction. Of special interest is the fundamental mode ($m = 1$) characterized by

$$u = u_1 = 2.4048. \tag{14}$$

Note that both eqs. (12) and (13) are frequency independent.

Thus, over the frequency range in which both conditions (1) and (7) are satisfied, the field distribution of an aperture illuminated by the HE_{11} mode is essentially frequency independent.[1,2] If, however, only condition (1) and not condition (7) is satisfied, then we must add[4] to the right-hand side of eq. (12) a component of the type (13), so that

$$E \approx J_0\left(\frac{r}{a}u\right)\mathbf{i}_x - \frac{\gamma - 1}{\gamma + 1}J_2\left(\frac{r}{a}u\right)(\cos 2\phi \mathbf{i}_x + \sin 2\phi \mathbf{i}_y), \tag{15}$$

where the factor $e^{-j\beta z}$ has been omitted. Both γ and u are functions of ka and X_s, and, therefore, they vary with frequency. If one develops γ,

u in power series of y and $1/ka$ one finds[4]

$$u = u_m \left\{1 - \frac{1}{2}\mathrm{y}\left(\frac{1}{ka}\right)\cdots\right\} \tag{16}$$

$$\gamma = 1 - u_m^2 \left\{\frac{\mathrm{y}}{2}\frac{1}{ka} - \frac{\mathrm{y}^2}{8}u_m^2\,(4 + u_m^2)\left(\frac{1}{ka}\right)^2\cdots\right\}. \tag{17}$$

2.2 Mode conversion in a conical horn[4]

Consider a conical horn of constant surface reactance and flare angle α, as shown in Fig. 1, from $z = z_1$ to $z = z_2$. If α is sufficiently small, and if the input of the horn is excited in the HE_{11} mode, then the resulting field inside the horn is very nearly a spherical wave[1,3] originating from the apex of the horn and given by

$$Ee^{-ikR}, \tag{18}$$

where E is given by eq. (15) and R is the distance from the apex of the horn. Since α is small,

$$R \simeq z + \frac{r^2}{2z}, \tag{19}$$

r being the radial distance from the axis and z the axial distance measured from the horn apex. From eq. 17, the parameter γ which appears in eq. (15) is a function of both y and ka; assume $|\mathrm{y}| \neq \infty, 0$. Then, since ka increases with z, we have from eq. (17) that γ varies with z, and therefore the field distribution (15) does not remain constant with z. This variation is accompanied by generation of unwanted modes, an effect that will be negligible only if α is sufficiently small.

To determine how small α should be, consider the special case $ka(z_1) \gg 1$ treated in Ref. 4. Let P_c be the total power converted from the desired mode into the HE_{11}' mode and let P_0 be the power incident at the input. Then, we find that for $z = z_2$

$$P_c = P_0 \times 3.393\,(10^{-3})\mathrm{y}^2 \tan^2\alpha |1 - e^{j\psi}|^2, \tag{20}$$

where

$$\psi = \frac{10.295}{\mathrm{y}\tan\alpha}\frac{\mathrm{y}}{ka(z_1)}\left(1 - \frac{a(z_1)}{a(z_2)}\right). \tag{21}$$

Therefore,

$$P_c \leqq P_0 \times 1.357(10^{-2})\mathrm{y}^2 \tan^2\alpha, \tag{22}$$

where the equality sign is attained for $\psi = (2\mathrm{n} + 1)\pi$. In the experiment, $\alpha = 4°$, in which case for $\mathrm{y} = 1$ we find $P_c \leqq 6.636 \times 10^{-5}$ (−41.8 dB), which is negligible for most practical purposes.

III. RADIATION CHARACTERISTICS[2,6,7]

Let the aperture of the horn be of sufficiently large diameter that the far field is simply proportional to the Fourier transform F of the aperture field. Also let α be so small that we can neglect the phase variation caused over the aperture plane by the variation of R in (18). Then, by taking the Fourier transform of eq. (15), we obtain for the field distribution at a great distance D from the aperture, for example, using the contour integral method of Ref. (4),

$$F = N_0(u,v)\mathbf{i}_x + \frac{\gamma - 1}{\gamma + 1} N_2(u,v)\ (\cos 2\phi \mathbf{i}_x + \sin 2\phi \mathbf{i}_y), \tag{23}$$

where

$$v = ka(z_2)\sin\theta, \tag{24}$$

$$N_k(u,v) = \frac{a^2}{v^2 - u^2}\left[vJ_k(u)J_1(v) - uJ_k(v)J_1(u)\right], \tag{25}$$

and ϕ, θ are spherical coordinates defined by $x = D\sin\theta\cos\phi$, $y = D\sin\theta\sin\phi$. Equation (23) gives, except for a factor independent of ϕ, θ, the far-field pattern. For small y/ka we have

$$u = u_1 = 2.4048.$$

In this case, from eqs. (23) to (25) the cross-polarization ratio C between the maximum value of $|E_y|$, which occurs for $v = 3.67$, and the maximum value of $|E_x|$, which occurs for $v = 0$, is given by

$$C^2 \equiv \frac{|E_y|^2_{\max}}{|E_x|^2_{\max}} = (0.26)^2\left(\frac{\gamma - 1}{\gamma + 1}\right)^2. \tag{26}$$

From eq. 17, the asymptotic value of C^2 for large ka is

$$C^2 \to 0.14\left(\frac{y}{ka}\right)^2. \tag{27}$$

If $ka \gg 1$, but y/ka is not small, C^2 has the behaviour of Fig. 2.

Equation (23) assumes that the aperture of the horn is illuminated by the HE_{11} mode. If, in addition to this mode, there is also some HE'_{11} mode of power P_c, then we have in addition to the component in (23), a component[4]

$$-e^{j\psi} \times \sqrt{\frac{P_c J_1^2(u)}{P_0 J_1^2(\bar{u})}}\, N_2(\bar{u},v)(\cos\phi\mathbf{i}_x + \sin\phi\mathbf{i}_y), \tag{28}$$

where P_c, P_0 are the powers carried by the two modes and ψ is their difference in phase for $z = z_2$. For $ka \gg 1$,

$$\bar{u} \approx u'_1 = 5.1356. \tag{29}$$

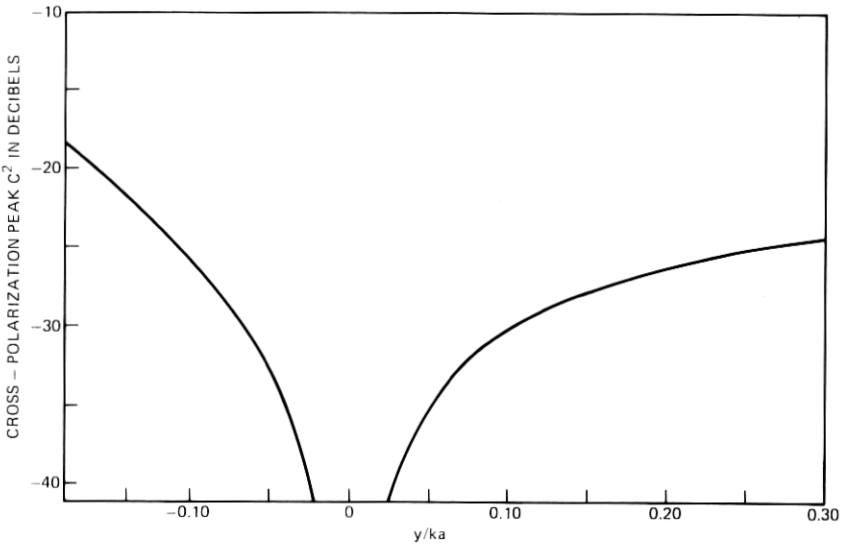

Fig. 2—Cross-polarization peak versus normalized surface susceptance.

Therefore, from eq. (25) with $J_2(\bar{u}) = 0$,

$$N_2^2(\bar{u},\upsilon) = \left(\frac{a^2\bar{u}}{\upsilon^2 - \bar{u}^2} J_2(\upsilon)J_1(\bar{u})\right)^2 \tag{30}$$

whose maximum value occurs for $\upsilon \approx 4.356$ and is

$$1.271 \times 10^{-3} \times a^4 J_1^2(\bar{u})\bar{u}^2. \tag{31}$$

Because of the component (28), we have for $\gamma = 1$ that the ratio C^2 between the maximum value of $|E_y|^2$, which now occurs for $\upsilon = 4.4$ and the maximum value of $|E_x|$ is

$$C^2 = 0.194 \frac{P_c}{P_0}. \tag{32}$$

Note from eq. (23) that the normalized radiation pattern of the HE_{11} mode for $ka \gg 1$ is simply given by

$$P(\theta) = \left[u^2 \frac{J_0(\upsilon)}{u^2 - \upsilon^2}\right]^2 \tag{33}$$

with $u = u_1 = 2.4048$ and $\upsilon = ka \sin\theta$. If θ_1 and θ_2 denote the values of θ for which $P(\theta) = 0.5$ and $P(\theta) = 0.1$, then from eq. (33)

$$ka \sin\theta_1 = 2.078 \text{ (3-dB point)} \tag{34}$$

and

$$ka \sin \theta_2 = 3.597 \text{ (10-dB point)}, \tag{35}$$

respectively.

IV. FEED DESIGN[2,4,9]

The feed of Fig. 1 is now described. Its measured characteristics are discussed in Section V. Let $\{\omega_2, \omega_1\}$ be the frequency range over which only the dominant mode, the HE_{11} mode, propagates at the input ($z \approx 0$). Let ω_0 be the frequency at which the surface reactance is infinite at the aperture; then

$$b(z_2) - a(z_2) \approx \frac{\lambda}{4}, \text{ at } \omega_0. \tag{36}$$

At the input, the ratio between the radii b and a is optimized for maximum ω_2/ω_1. This is shown in Appendix A to require

$$\frac{b(0)}{a(0)} = \frac{7.0155}{3.8317} = 1.8309. \tag{37}$$

Then*

$$\frac{\omega_2}{\omega_1} = \left(\frac{\omega_2}{\omega_1}\right)_{\text{MAX}} = 1.6839, \tag{38}$$

and the surface reactance can be shown to vanish for $\omega = \omega_2$,

$$y = \infty \text{ for } z = 0, \text{ at } \omega = \omega_2. \tag{39}$$

In the experiment, the frequency ω_1 was chosen equal to 19 GHz, which gives $\omega_2 = 28.8$ GHz, $a(0) = 0.556$ cm, and $b(0) = 1.161$ cm, as we obtain from eqs. (37) and (38) and the condition

$$kb = 7.0155 \text{ at } \omega = \omega_2, \tag{40}$$

shown by Fig. 9 of Appendix A.

From Fig. 1 the feed consists of two parts joined at $z = z_1$. From $z = 0$ to $z = z_1$, the outer radius is kept constant, so the cutoff frequency of the HE'_{11} mode remains constant, as shown in Appendix A, where the relations between a, b and the cutoff frequencies of the various modes of eqs. (12) and (13) are derived. Note that from $z = 0$ to $z = z_1$ the radius a increases, which implies that at any given frequency the surface reactance decreases with z. The importance of this requirement was first realized by Bryant[8]. From $z = z_1$ to the aperture, the surface reactance remains constant with z. The frequency ω_0 at which it is infinite was chosen in the experiment

* To put this ratio in perspective, the highest frequency of the 6-GHz (TH) common carrier band is 1.732 times the lowest frequency of the 4-GHz (TD-2) band; similarly, for the 18- and 30-GHz bands, the ratio is 1.695.

$$\omega_0 = 1.21\,\omega_1. \tag{41}$$

Over the frequency range $\{\omega_1, \omega_2\}$ only the HE_{11} mode is excited at the input, other modes being cut off. Therefore, since the variations of $a(z)$ and $b(z)$ from the input to the aperture in Fig. 1 are sufficiently gradual to ensure negligible generation of unwanted modes, we have that the aperture is essentially illuminated by a single mode, the HE_{11} mode, over the above frequency range. The radiation characteristics for $\omega_1 < \omega < \omega_2$ are, therefore, given accurately by eq. (23) with $a = a(z_2)$ and u given by eq. (16) for $m = 1$.

From eq. (39), the input surface reactance vanishes at ω_2. Therefore, since the corrugated waveguide is connected at the input to a smooth waveguide of the same diameter, the input reflection is essentially zero at $\omega = \omega_2$. For $\omega \neq \omega_2$, however, there is a reflection which, as we shall see in Section V, is given accurately by

$$|\rho|^2 = \left(\frac{\beta_1 - \beta_1'}{\beta_1 + \beta_1'}\right)^2, \tag{42}$$

where β_1 is the propagation constant of the TE_{11} mode and β_1' is that of the HE_{11} mode. Equation (42) is derived in Ref. 4.

At frequencies higher than ω_2, some of the incident power is converted into the HE_{11}' mode. If P_c denotes the converted power and P_0 denotes the incident power, then

$$\frac{P_c}{P_0} \approx \left[\frac{1}{a(\beta_1 - \beta_2')y}\right]^2 \frac{\beta_1}{\beta_2'(u^2 - 1)}, \tag{43}$$

where $u = 1.841$ and β_2' is the propagation constant of the HE_{11}' mode. Some of the incident power is also converted into the TM_{11} mode of the smooth waveguide. If P_c' denotes this power, which is reflected by the junction, we have[4]

$$\frac{P_c'}{P_0} \approx \frac{(\beta_2 - \beta_2')^2}{(\beta_1 + \beta_2')^2 u^2 - 1} \frac{\beta_2 \beta_1}{k^2} \frac{1}{}, \tag{44}$$

where β_2 is the propagation constant of the TM_{11} mode. The above coupling equations are derived in Ref. 4 assuming $|y| \gg 1$.

In the experiment described in the following section, the corrugated waveguide is connected at the input to a smooth waveguide whose radius gradually increases from a relatively small value a' to the final value $a(0)$. The initial value a' is sufficiently small so that the TM_{11} mode is cut off and, as a consequence, the power P_c' is reflected back towards the junction where it is converted into the HE_{11}' mode of the corrugated waveguide. The total power converted into the HE_{11}'mode is thus in general different from P_c. It varies approximately between the two values

$$(\sqrt{P_c} - \sqrt{P_c'})^2 \text{ and } (\sqrt{P_c} + \sqrt{P_c'})^2, \tag{45}$$

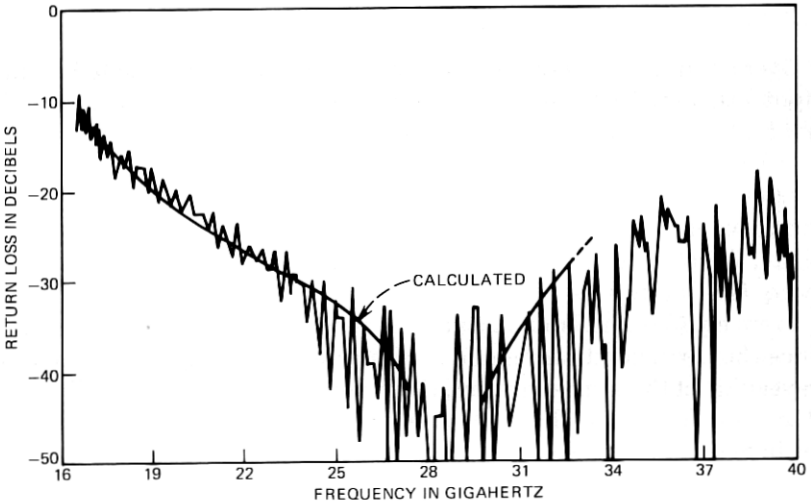

Fig. 3—Return loss of corrugated horn of Fig. 1 vs frequency.

depending on the phase angle of the TM_{11} mode incident on the junction.

V. EXPERIMENT

A corrugated feed of the dimensions shown in Fig. 2 was built using a technique described in Appendix C. Its measured reflection coefficient agrees* very well with eq. (42), as shown in Fig. 3. Its radiation characteristics are shown in Figs. 4 through 6. From 17.5 GHz to 32 to GHz, the radiation patterns are in good agreement with eq. (33), as shown in Fig. 4, which compares eq. (33) with two measured patterns of $|E_x|^2$ in the plane $\phi = 45°$. Furthermore, from 17.5 GHz to 32 GHz, there is little difference between the patterns of $|E_x|^2$ in the two principal planes ($\phi = 0$ and $\phi = 90°$) and the pattern for $\phi = 45°$. The difference is altogether negligible at $\omega_0 = 23$ GHz, which is the frequency for which $y = 0$ at the aperture. Figures 5 and 6 show a few examples of patterns measured in the two principal planes. The variations with frequency of the beamwidths $2\theta_1$ and $2\theta_2$ (respectively, the 3-dB and 10-dB beamwidths) agree very well with eqs. (34) and (35), as shown in Fig. 7, where the measured beamwidths in the plane $\phi = 45°$ are compared with the calculated values.

Finally, the cross-polarized component E_y is very small over the frequency range of eq. (2), as shown in Fig. 8. For $\omega > 28.8$ GHz, however,

* Note that the measured reflection coefficient includes a small reflection due to a transition from rectangular to circular waveguide, which was connected at the input of the feed during the measurement.

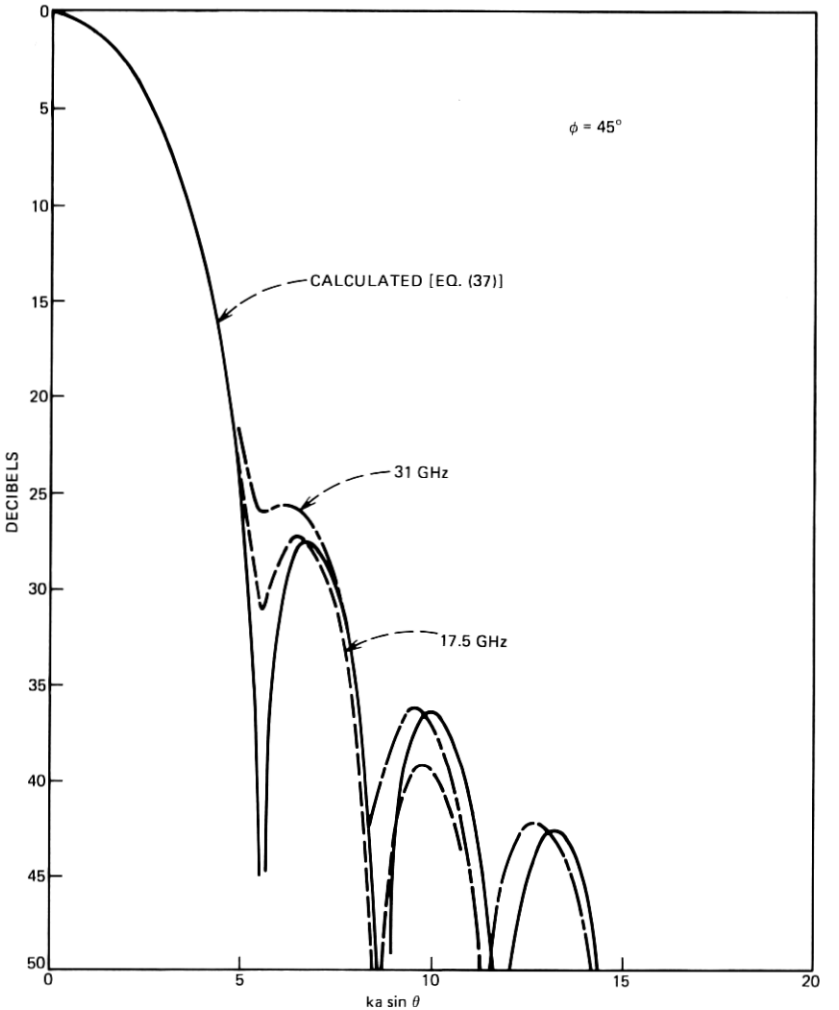

Fig. 4—Calculated and measured radiation patterns vs normalized angle at $\phi = 45°$.

the normalized peak C^2 of E_y increases rapidly with frequency as expected because of the HE'_{11} mode, which is excited at the input for $\omega >$ 28.8 GHz. The solid curves and the dashed curves in Fig. 8 correspond to eqs. (27) and (43), respectively. The agreement with the measurements is satisfactory, taking into account that eq. (43) is not expected to give exactly the total power converted into the HE'_{11} mode, for several reasons. In the first place, eq. (43) assumes a very large number of disks per wavelength,

$$h \ll \lambda,$$

whereas in the experiment, $h \approx 0.137\lambda$ at 30 GHz; the effect of a finite number of teeth is briefly discussed in Appendix B. In the second place, eq. (43) assumes that only the TE_{11} mode is incident at the input, whereas in practice also the TM_{11} mode is incident, for the reason pointed out in Section IV. The total power carried by the TM_{11} mode is approximately given by eq. (44).

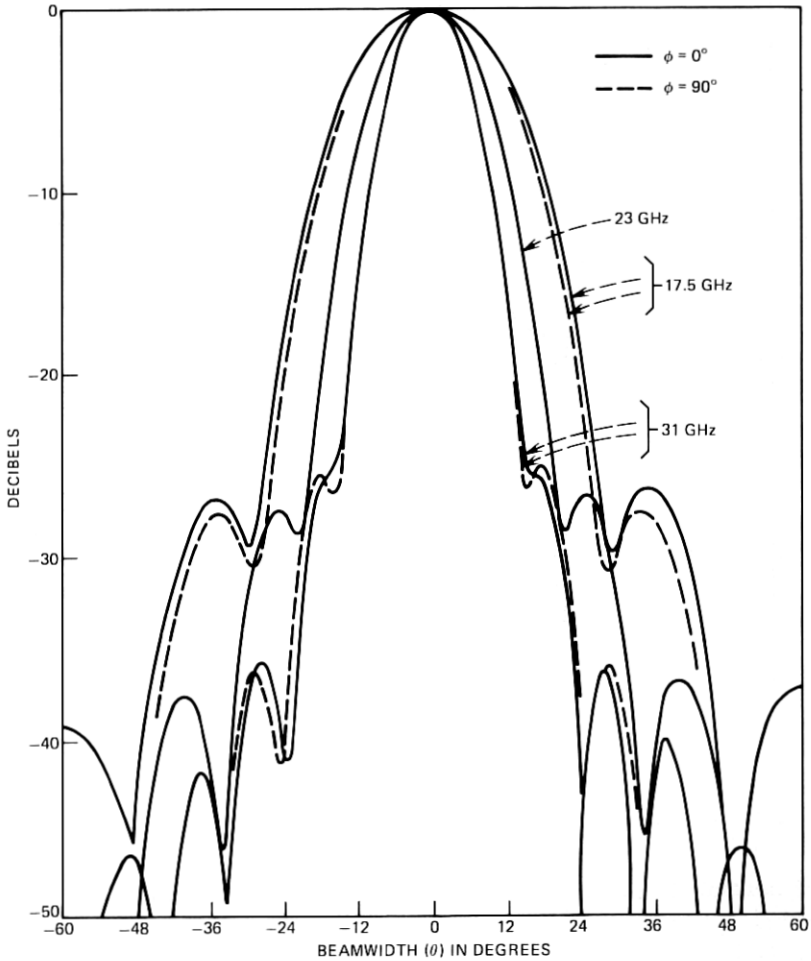

Fig. 5—Measured radiation patterns at $\phi = 0°$ and $\phi = 90°$ (principal planes).

Note, finally, that even if the total power converted into the HE'_{11} mode is calculated accurately, to determine the resulting cross-polarization peak C^2, the difference in phase between the HE_{11} and HE'_{11} modes must be determined.

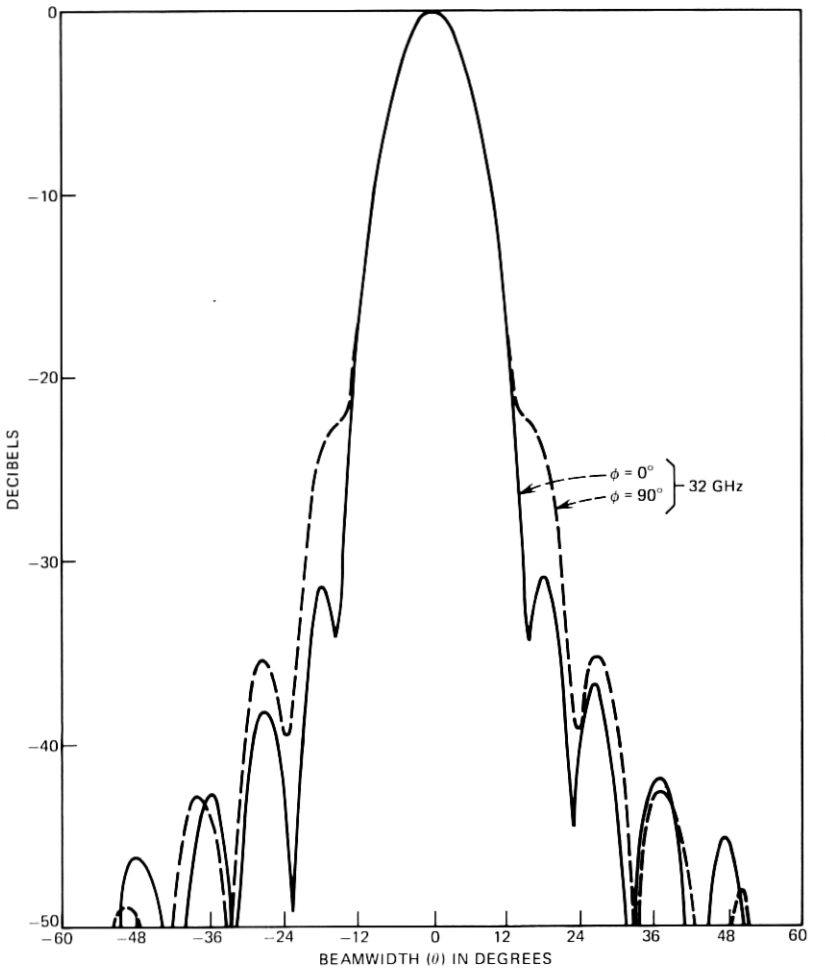

Fig. 6—Measured radiation pattern at $\phi = 0°$ and $\phi = 90°$ for 32 GHz (effect of HE'_{11} mode on pattern symmetry is evident at upper frequency limit of operation).

VI. CONCLUSIONS

Using a novel fabrication technique, described in Appendix C, which can be applied at very high frequencies, a corrugated feed of small flare angle was fabricated. Its input reflection, found to be given accurately by the simple formula

$$|\rho|^2 = \left(\frac{\beta_1 - \beta_1'}{\beta_1 + \beta_1'}\right)^2,$$

remained less than −30 dB from about 24 to 32 GHz. Over the frequency range $\omega_1 < \omega < \omega_2$, the far field was essentially polarized in one direction;

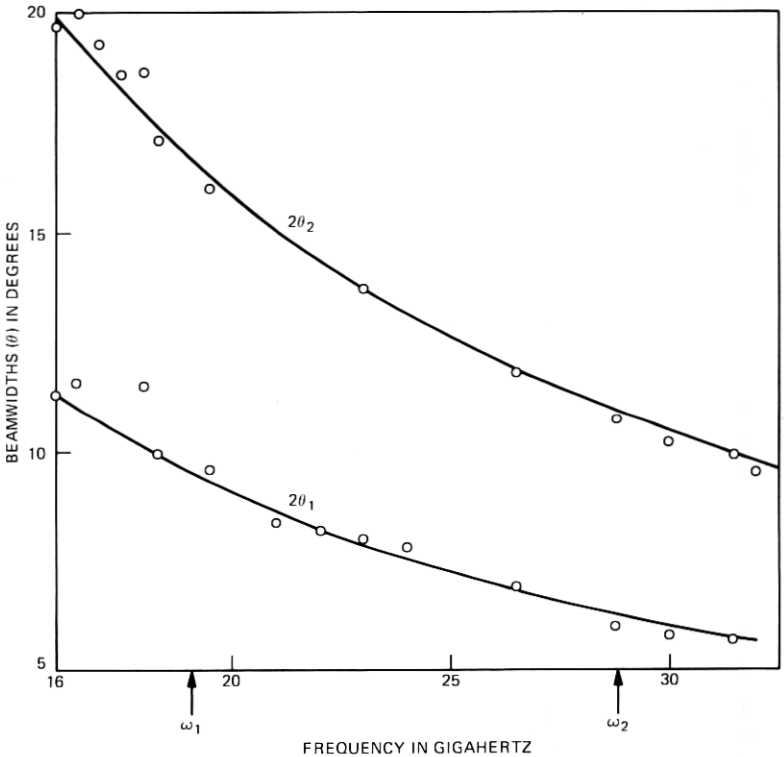

Fig. 7—Calculated and measured 3-dB and 10-dB beamwidths.

its pattern is simply given by

$$P(\theta) = \left(u^2 \frac{J_0(v)}{u^2 - v^2}\right)^2.$$

At frequencies higher than 28.8 GHz, the far field contained a cross-polarized component, as predicted by the theory of Ref. 4.

It was shown that a maximum bandwidth, expressed as the ratio ω_2/ω_1, of about 1.68 can be achieved for the type of corrugations considered here. By using the corrugations of Ref. 10, which, however, are difficult to realize at high frequency, greater values of ω_2/ω_1 may be achieved.

Both the input reflection and the cross-polarization ratio can be improved by increasing the thickness t of the disks at the input. Curves of $|\rho|^2$ and C^2 as a function of frequency for different values of t/h are given in Fig. 2 of Ref. 4. In the experiment, t/h was kept constant for reasons of simplicity, since our main concern was to verify the results of Sections II through IV and of Refs. 1 and 4, and to demonstrate the feasibility of the fabrication technique described in Appendix D.

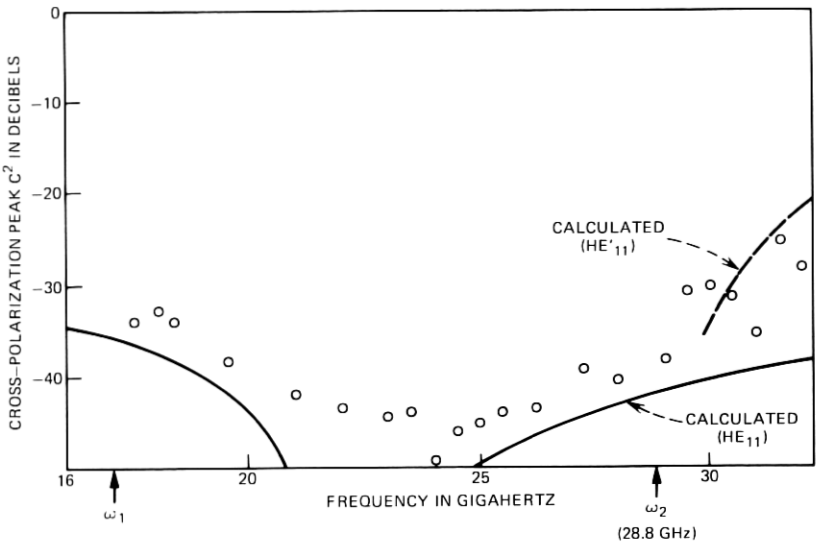

Fig. 8—Calculated and measured cross polarization; these are maximum values of cross polarization (see Section III, eq. 26).

ACKNOWLEDGMENT

The author wishes to acknowledge the assistance of W. E. Legg who carried out the measurements.

APPENDIX A

Cutoff Frequencies of the HE_{lm} and HE'_{lm} Modes

To determine eqs. (37) to (40) it is necessary to establish the relation between a, b and the cutoff frequencies of the various modes of eqs. (12) and (13). Assume the thickness of the disks is very small. Consider first the cutoff frequencies ω_{cm} of the HE_{lm} modes, which are characterized for large ka by the field distribution of eq. (12). In the vicinity of the cutoff frequency ω_{cm}, we have, for any one of the above modes,

$$\cos \theta_m = 0, \tag{46}$$

where $k \cos \theta_m$ is the propagation constant in the z direction,

$$\cos \theta_m = \sqrt{1 - \frac{u_m^2}{(ka)^2}}. \tag{47}$$

For $\omega \cong \omega_{cm}$, we can show[2,4] that the mode degenerates into either a TE mode or a TM mode according to the following rule:

$$\left.\begin{array}{l}\text{TE mode, if } y > 0,\\ \text{TM mode, if } y < 0,\end{array}\right\}. \tag{48}$$

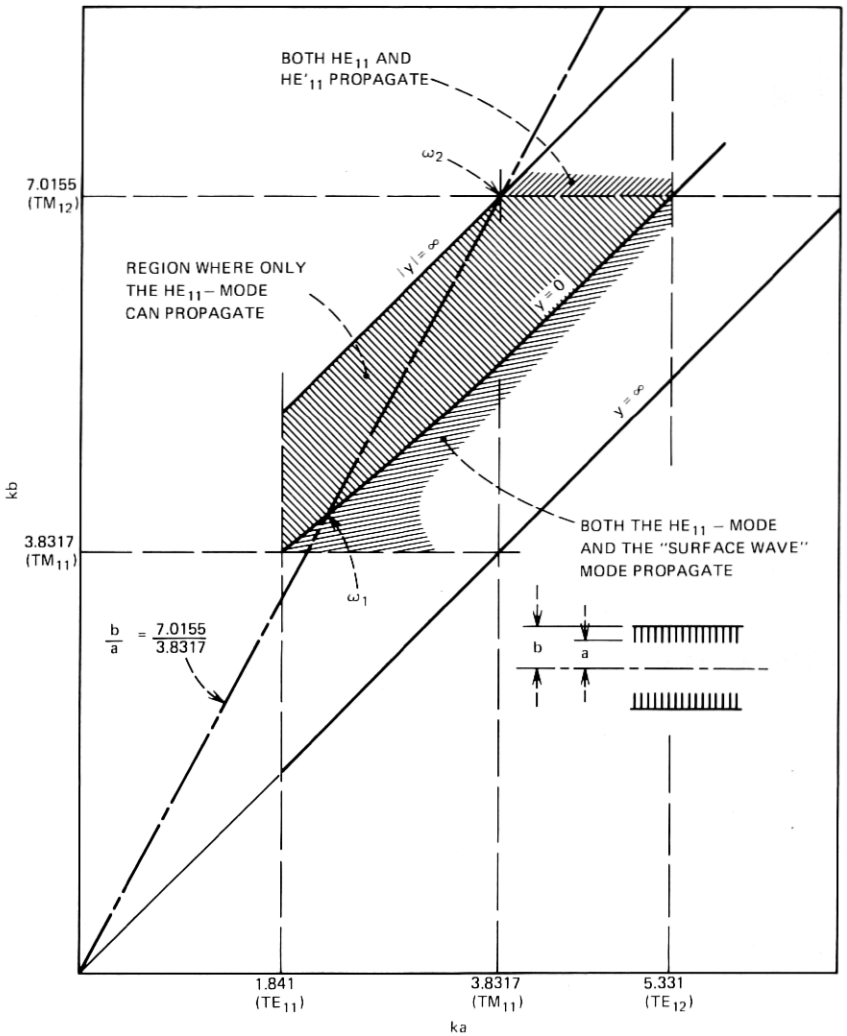

Fig. 9—Region where only the HE_{11} mode propagates. Note: As ω varies for a given a, b, a point ka, kb moves along a straight line through the origin.

In the former case, since the only nonzero component of the magnetic field of a TE mode near cutoff is H_z, we have $H_\phi = 0$, and therefore the second of the two boundary conditions (6) can be ignored, which implies that ω_{cm} is independent of y. The corrugated waveguide can be replaced, therefore, with a smooth waveguide of the same diameter whose cutoff frequencies for the TE modes are given by the roots of $J_1'(ka)$,

$$J_1'(ka) = 0 \text{ for } \omega = \omega_{cm} \ (y > 0). \tag{49}$$

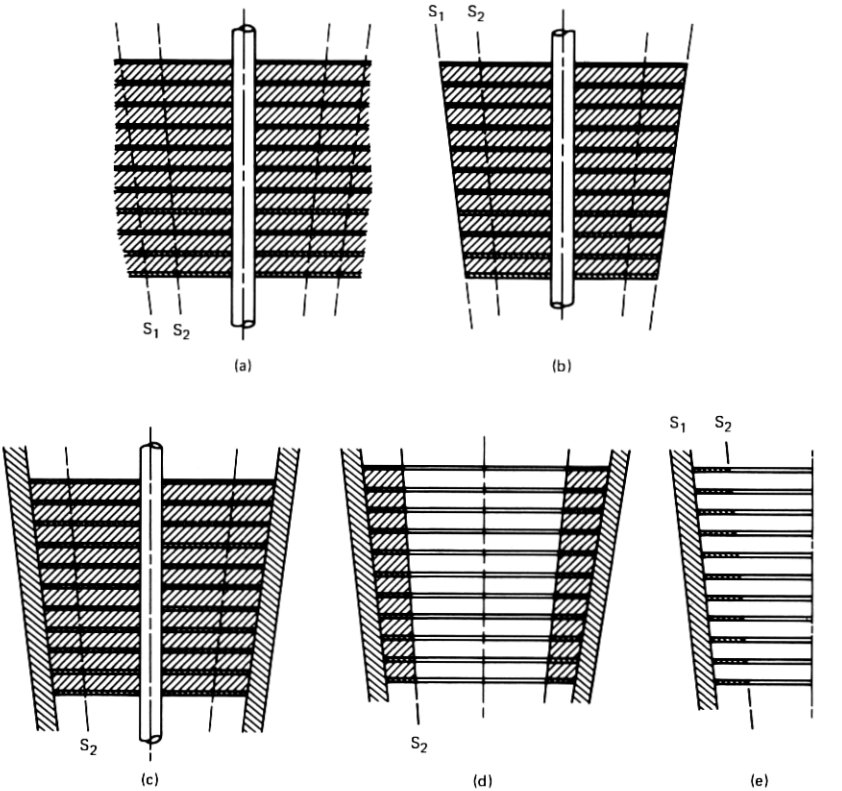

Fig. 10—Aluminum and brass disks assembled on mandrel. (a) Before machining. (b) After machining exterior surface. (c) With electroformed wall of copper. (d) After machining interior surface. (e) After etching away aluminum disks.

In the latter case, $y < 0$, the only component of the electric field for $\omega \simeq \omega_{cm}$ is E_z and, therefore, the very thin disks can be removed without affecting the field. The cutoff frequencies therefore coincide with those of the TM modes in a smooth waveguide of radius b, and are given by the roots of $J_1(kb)$,

$$J_1(kb) = 0 \text{ for } \omega = \omega_{cm}, \ (y < 0). \tag{50}$$

Analogous considerations[4] are valid for the HE'_{lm} modes, except that now, instead of the rules (48),

$$\left.\begin{array}{l} \text{TM mode, if } y > 0, \\ \text{TE mode, if } y < 0, \end{array}\right\}, \tag{51}$$

and therefore the cutoff frequencies ω'_{cm} are given by the conditions

$$\begin{aligned} J'_1(ka) &= 0 \text{ for } \omega = \omega'_{cm}, \text{ if } y < 0 \\ J_1(kb) &= 0 \text{ for } \omega = \omega'_{cm}, \text{ if } y > 0. \end{aligned} \tag{52}$$

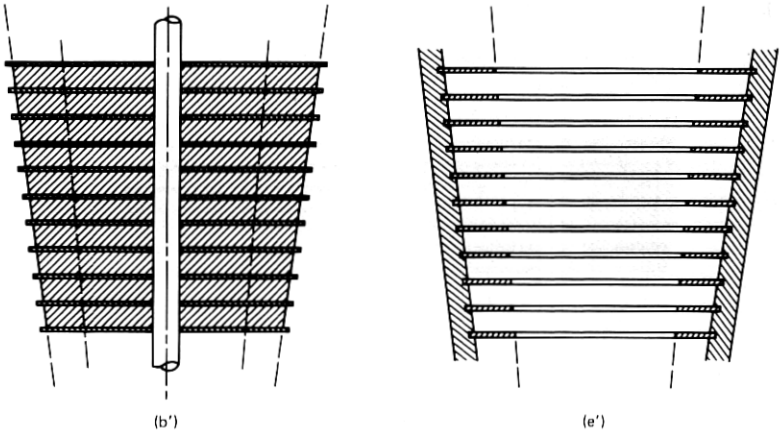

Fig. 11—Modification of assembly to obtain strong attachment to teeth of electroformed wall.

These results are illustrated by the diagram of Fig. 9 showing in the ka,kb plane the region* where only the HE_{11}-mode can propagate. We can see that ω_2/ω_1 is maximum when $b/a = 7.0155/3.8317 = 1.8309$, in which case $\omega_2/\omega_1 = 1.6839$, as pointed out in Section I before eq. 2.

APPENDIX B

Effect of a Finite Number of Teeth Per Wavelength

In Section IV, we assumed an infinite number of teeth per wavelength—i.e.,

$$h \ll \lambda,$$

a condition which seldom holds in practice. For instance, in the experiment

$$h > 0.13716\lambda$$

for $\omega > 30$ GHz. The effect of a finite number of teeth is not difficult to evaluate approximately if

$$ka \gg 1,$$

In this case, in fact, the field in the vicinity of the corrugations can be considered to be locally the field of a plane wave reflected by a corrugated plane tangent to the actual corrugated surface. The angle of incidence

* In Fig. 9 we have not indicated a region for $kb < 3.8317$ where mode propagation can occur, since that region is of no interest to us here. (The HE_{11} mode is cut off for $kb < 3.8317$).

is $90° - \theta_1$, where

$$\cos \theta_1 = \frac{\beta_1}{k}.$$

Thus, from Ref. 9, we find that a corrugated waveguide of radius $a \gg \lambda$ with a finite number of teeth is equivalent to one with $h \ll \lambda$, but with slightly larger inner radius a',

$$a' \simeq a + \frac{\ln 2}{\pi} h,$$

and the same outer radius b. Although this result is strictly valid only if $a \gg \lambda$, measurements[11] have shown that it is valid approximately even for $ka \simeq 4$.

APPENDIX C

Fabrication Technique

Even if the aperture of a feed is illuminated by a single mode, the far field contains a cross-polarized component with amplitude proportional to [eqs. (4), (5), and (27)]

$$\left|\frac{y}{ka}\right| = \left|\frac{1}{(1 - t/h)\, ka \tan kl}\right|. \tag{53}$$

To minimize this cross-polarized component, it is important that the thickness t of the disks be much smaller than their separation h,

$$t \ll h. \tag{54}$$

Since h is always appreciably smaller than $\lambda/4$, and since typically the depth l of the grooves is not much different from $\lambda/4$, condition (54) implies

$$t \ll \lambda/4 \tag{55}$$

$$t \ll l. \tag{56}$$

Corrugated feeds are difficult to fabricate. When a corrugated feed is electroformed, a mandrel of aluminum or other material is first prepared, and then the corrugated feed is electroformed around the mandril, which is then removed with a solvent. However, at high frequencies, say at frequencies higher than about 10 GHz, condition (55) demands that t be very small (much less than 0.318 cm). Then, taking into account (56), the above technique cannot be used.

Figures 10 and 11 illustrate a technique that can be used at very high frequencies, as high as 100 GHz, and which allows very small thicknesses t to be realized. First a set of disks of aluminum and brass is assembled, as shown in Fig. 10a, to form a single block whose outside surface is then

machined as shown in Fig. 10b. The central rod shown in Figs. 10a and b defines the axis of the corrugated waveguide. The surface S_1 corresponds to the bottom of the grooves, as shown in Fig. 10e. The thickness of the brass disks is t and, that of the aluminum disks, $h - t$. After the surface S_1 is machined, a wall of copper (or other metal) is electroformed, as shown in Fig. 10c. The central rod is then removed, and the inside surface S_2, which corresponds to the tops of the grooves (see Fig. 10e), is machined as shown in Fig. 10d. Finally, the aluminum is removed with a solvent and the final product is the corrugated waveguide of Fig. 10e. An important feature of this technique is that the two surfaces S_1 and S_2 can be machined very accurately.

If the brass disks are too thin, their mechanical adherence to the copper wall in Fig. 10e may not be satisfactory. In this case, we may modify the above procedure by adding, after step b, an extra step b′ in which the brass disks of Fig. 10b are replaced with disks of somewhat larger diameter, as shown in Fig. 11b′. The exact dimensions of the new disks are not important. The final result, after the aluminum is removed, is shown in Fig. 11e′. The disks are now embedded in the copper wall.

REFERENCES

1. B. MacA. Thomas, "Bandwidth Properties of Corrugated Conical Horns," Electron. Lett., *5*, No. 22 (October 30, 1969), pp. 561–563.
2. P. J. B. Clarricoats and P. K. Saha, "Propagation and Radiation Behaviour of Corrugated Feeds; Part I—Corrugated Waveguide Feed," Proc. IEE, *118*, No. 9 (September 1971), pp. 1167–1176.
3. P. T. B. Clarricoats and P. K. Saha, "Propagation and Radiation Behaviour of Corrugated Feeds; Part 2—Corrugated Conical-Horn Feed," Proc. IEE, *118*, No. 9 (September 1971), pp. 1177–1186.
4. C. Dragone, "Reflection, Transmission, and Mode Conversion in a Corrugated Feed," this issue, pp. 835–868.
5. V. H. Rumsey, "Horn Antennas With Uniform Power Patterns Around Their Axes," IEEE Trans. Ant. Propag., *AP-14*, No. 5 pp. 656–658.
6. H. C. Minnett and B. MacA. Thomas, "A Method of Synthesizing Radiation Patterns with Axial Symmetry," IEEE Trans. Ant. Propag., AP-14, No. 5 (September 1966), pp. 654–656.
7. M. S. Narasimlian and B. V. Rao, "Hybrid Modes in Corrugated Conical Horns," Electron. Lett., *6*, No. 2 (January 22, 1970), pp. 32–34.
8. G. H. Bryant, "Propagation in Corrugated Waveguides," Proc. IEE, *116*, No. 2 (February 1969), pp. 203–213.
9. R. E. Collin, *Field Theory of Guided Waves*, New York: McGraw-Hill, 1960.
10. Y. Takeichi, T. Hashimoto, and F. Takeda, "The Ring-Loaded Corrugated Waveguide," IEEE Trans. Microw. Theory Tech., *MTT-19*, No. 12 (December 1971), pp. 947–949.
11. M. J. Gans, private communication.